JOINT EUROPEAN TORUS

JET–P(92)36

A.L. Colton, P.J. Cripwell, G.J. Kramer, A.C.C. Sips
and JET Team

Measurements of ELMs and Associated Fluctuations with the Multichannel Reflectometer System

Measurements of ELMs and Associated Fluctuations with the Multichannel Reflectometer System

A.L. Colton[1], P.J. Cripwell, G.J. Kramer[2], A.C.C. Sips
and JET Team*

JET-Joint Undertaking, Culham Science Centre, OX14 3DB, Abingdon, UK

[1]Association Euratom-Risp National Laboratory, Denmark.
[2]FOM Institute for Plasma Physics 'Rijnhuizen', The Netherlands
** See Annex*

Preprint of Paper to be submitted for publication in
Proceedings of the IAEA Workshop on Microwave Reflectometry

MEASUREMENTS OF ELMS AND ASSOCIATED FLUCTUATIONS WITH THE MULTICHANNEL REFLECTOMETER SYSTEM

A.L. Colton[1], P.J. Cripwell, G.J. Kramer[2] and A.C.C. Sips

JET Joint Undertaking, Abingdon, OXON OX14 3EA, UK
1) Association Euratom - Riso National Laboratory, DK
2) FOM Institute for Plasma Physics 'Rijnhuizen', NL

Abstract

The potential and limitations of JET's Multichannel Reflectometer System for studying ELMs have been evaluated. Two new methods for calibrating fixed frequency data have been developed to cope with the problems caused by ELMs. Results on both the temporal and radial evolution of the ELMs and associated fluctuations are presented, and the significance of the relative proportion of phase and amplitude fluctuations is discussed.

Introduction

Edge Localised Modes (ELMs) are characterised by bursts of D_α emission during the H-mode and the L-H transition. The ELMs are generally associated with a temporary decrease in confinement, which results in increased particle and energy transport across the last closed flux surface (lcfs), and consequently increased D_α emission. As the ELMs thus reduce both the plasma and impurity densities in the edge region, they have potential for controlling the density and prolonging the H-mode.

The plasma region of interest is the edge region spanning 20 cm inwards from the lcfs, ie. at relative minor radius $\rho = 0.8 - 1.0$. The ELMs occur on a timescale of a few ms, and they are associated with fluctuations over a wide frequency range, up to at least 100 kHz. The interval between ELM's varies from 0.5 ms for a series of small ELMs occuring during the L-H transition, to seconds for large singular ELM's later in the H-mode.

The Multichannel Reflectometer System at JET.

The multichannel reflectometer system probes the plasma along the horizontal midplane with microwaves polarized in the ordinary mode. It employs separate launch and reception antennas, oversized wave guides for transmitting the microwave power to and from the antennas, Gunn oscillators as sources and a heterodyne detector system [1]. There are twelve discrete probing frequencies in the range 18 - 80 GHz corresponding to critical electron densities from 4×10^{18} m^{-3} to 8×10^{19} m^{-3}.

During an H-mode the density profile is relatively constant across most of the plasma, decreasing steeply in the edge region. Thus a spatial resolution of around 5 cm or less is needed to obtain quantitative measurements of the edge density profile. The reflectometer has the advantage that it measures the radial positions of layers of fixed density. Most of the reflection points are found where the density gradient is steepest, resulting in a good spatial resolution in the edge region.

The reflectometer has two independent arrays of detectors:

1) The coherent detectors measure a combination of changes in phase caused by movements of the reflecting layer and changes in the amplitude of the reflected wave, equivalent to homodyne detection. Frequency spectra of the density related fluctuations can be computed from the data; the maximum sampling rate is 500 kHz.
2) The fringe counters measure the phase part of the signal, $\phi(t)$, in units of fringes (one fringe is equivalent to a phase change of 2π radians). The resolution is 1/128 fringe corresponding to movements of the reflecting layers of $\simeq$0.2 mm. In order to eliminate the effects of high frequency density fluctuations the fringe counter data is filtered at a bandwidth of 3 kHz. Apparent 'jumps' in the measured phase still occur occasionally, mostly caused by momentary loss of signal from the plasma arm. These phase jumps are eliminated by taking the time derivative of the signals and removing the spikes in $d\phi/dt$ corresponding to the jumps.

The reflectometer has two modes of operation: fixed frequency, for monitoring the relative movements of the critical density layers; and narrow band swept frequency, for generating density profiles. In the latter case, the frequency of each source is swept over a narrow band (typically 100 MHz). The resultant change of phase is measured, at a rate of around 25 samples/sweep. In order to eliminate phase changes caused by movements of the reflecting layers during the sweep the reflectometer employs a sweep/dwell technique. A number of fixed frequency samples is taken in the dwell periods between each frequency sweep [1]. These measurements are used to reconstruct a baseline corresponding to the movements of the reflecting layers. This can then be separated from the phase changes caused by the frequency sweeps. Alternatively the baseline can be used as fixed frequency data.

Calculation of Density Profiles.
The phase delay ϕ of an ordinarily polarised wave of frequency F_c reflected from the cut-off layer is [2]:

$$\phi_c = \frac{4\pi F_c}{c}\int_{R_c}^{R_{out}} \mu(n(R))\,dR - \frac{\pi}{2} \quad , \quad \mu = \left(1 - \frac{n(R,t)}{n_c}\right)^{1/2} \tag{1}$$

where n(R) is the electron density at radial position R, $n_c = F_c^2 4\pi^2\varepsilon_0 m_e/e^2$ is the critical density, R_c is the position of the reflecting layer, R_{out} is a reference position outside the plasma edge, and μ is the refractive index.

From (1) it can be seen that changes in the phase delay can be caused by changes in both the density profile and the reflectometer frequency. Self-calibrated density profiles can be calculated from measurements of the change in phase with frequency, $d\phi_c/dF_c$, using an Abel inversion technique [1].

Measurements of $\phi_c(t)$ at fixed frequency give the relative movements of the critical density layers. Several techniques can be employed to convert these into density profiles, all of which require a reference density profile for calibration.

Linear Method:
The density profile is approximated by a linear model with a constant gradient, $n_0/\Delta R$, from the plasma edge R_{edge} to a position $R_{edge} - \Delta R$ in the plasma, and a constant value

n_0 throughout the rest of the plasma. Inserting this model in (1) gives the density gradient and the edge position:

$$\frac{\phi_c + \phi_{0,c}}{\frac{4\pi}{c} F_c} = \frac{2}{3} \frac{\Delta R}{n_0} n_c + R_{out} - R_{edge} \tag{2}$$

The multichannel reflectometer provides simultaneous measurements of ϕ_c at several critical densities n_c. With these data the density gradient and plasma edge position can be calculated from (2) employing linear regression.

In order to calculate the phase constants $\phi_{0,c}$, a set of values for the density gradient and edge position is obtained from a reference density profile. These are then inserted in (2) to give $\phi_{0,c}$ for each n_c.

Piecewise Linear Method:

The density profile is assumed to be linear between each critical density n_i at radial position R_i, with gradient $\Delta n_i/\Delta R_i$ between n_i and n_{i-1}. Assuming that the plasma edge position R_{edge} is known, the position of each subsequent critical density n_c is given by:

$$R_c = R_{c-1} - \sqrt{\frac{n_c}{\Delta n_c}} \left[\frac{3}{2} (\phi_{c,nor} - R_{out} + R_{edge}) + n_c \sum_{i=1}^{c-1} \frac{\Delta R_i}{\Delta n_i} (\mu_i^3 - \mu_{i-1}^3) \right] \tag{3}$$

Here, $\Delta R_i = R_i - R_{i-1}$, $\Delta n_i = n_i - n_{i-1}$, $\phi_{c,nor} = \frac{c}{4\pi} (\phi_c - \phi_{0,c})$:ef, :f.$R_0 = R_{edge}$ and $n_0 = 0$.

In order to calculate the phase constants $\phi_{0,c}$ a reference density profile is used. The positions of the critical densities are obtained from the reference profile. Inserting these in (3) then gives $\phi_{0,c}$ at each critical density.

Fringe Counter Phase Measurements during ELMs.

The narrow band sweep profiles are generated at a rate of one per sweep/dwell period ie. with a temporal resolution of 15-30 ms, and it is only possible to generate profiles when the positions of the reflecting layers do not change abruptly during the sweep. The density evolution during ELMs is thus too fast to be studied using narrow band sweep profiles.

The temporal resolution of the fixed frequency phase data is $\simeq$0.3 ms, fast enough to resolve the ELMs. The fixed frequency phase data have the following limitations:

- 3 kHz filters limit the movement of the reflecting layers that can be observed; the maximum observable radial velocity is $\simeq$10 m/s.
- All methods of generating profiles from fixed frequency data require a reference density profile for calibration. However it is usually possible to use a narrow band swept profile from the reflectometer, independently of other diagnostic systems.
- Since the fringe counters measure the total phase change, a fixed frequency profile will be corrupted by any phase 'jumps' in the period between the time of the reference profile and the time of interest. Thus a new reference profile must be used in each period of good data between phase jumps.

The linear method depends on linear regression of data from several channels. This results in a fairly good tolerance of phase jumps on any single channel. Furthermore the

error on the linear fit at any given time can be calculated. This is due to phase jumps and to changes in the profile shape, in the period since the reference profile time. As the change in profile shape during ELMs is small, the error gives an estimate of the data corruption caused by phase jumps during the ELMs. Comparisons show that the linear approximation to the density profile is usually good in the edge region, particularily during the H-mode [3].

The piecewise linear method was developed to overcome the limited radial resolution of the linear method. It allows the movement of each critical density layer to be calculated individually. Thus the radial propagation of a density pulse can be resolved. The main disadvantage is the lower tolerance for phase jumps, as the calculation of each critical position is corrupted by errors in the phase data at any lower density. Furthermore it is also necessary to obtain the plasma edge position from another diagnostic.

Edge Density Gradient

The linear method has been used to calculate the average density gradient in the edge region. In fig.1 the top traces show the density gradient during one medium and two small ELMs. The calculation is based on a reference profile in the beginning of the period. The uncertainty on the gradient increases during each ELM. The reason for this is most likely that the reflecting layers move faster than can be observed by the fringe counters due to the 3 kHz filtering. The maximum velocity that can be resolved by the filters is $\simeq$10 m/s, whereas a propagation velocity of $\simeq$13 m/s is observed by comparison of several channels.

The middle trace in fig.1 shows the electron temperature gradient, which decreases sharply during the ELM. The relative decrease is around 10 %, of the same order as the observed decrease in density gradient. The timescale of the decrease is however much shorter. This is partly instrumental as the density gradient is calculated as an average over the whole edge region, disguising the radial evolution. Part of the difference may also be physical as the heat transport is faster than the particle transport [1].

Radial Density Evolution

In fig.2 a contour plot of the critical densities against radius and time generated by the piecewise linear method is shown, during the three ELMs of fig.1. The larger ELM originates between $n = 1.4x10^{19} - 2x10^{19}m^{-3}$, causing an outward propagating density pulse. The propagation velocity is found by calculating the time delay between the pulse on different density contours, thus overcoming the limited time response of each channel due to the 3 kHz filters. The propagation velocity is 13 m/s, that is $\simeq$25 % larger than the local diffusion velocity [3]. In the edge region inside $n = 1.7x10^{19}m^{-3}$ a density decrease is observed spreading inwards.

The low amplitude ELMs start further inwards, at $n = 2x10^{19} - 3x10^{19}m^{-3}$. They also generate outward propagating density pulses, but these appear to die away before they reach the plasma edge and cause a D_α burst.

Coherent Detector Fluctuation Data

The coherent detectors measure fluctuations in both amplitude, A, and phase, ϕ, of the reflected signals. The reflected signal is given by:

$$S(t) = A(t)\cos(\phi(t)) \quad (4)$$

The fluctuation level of the signal depends on the value of ϕ; if $\phi \simeq \pm \pi/2$ the fluctuations in phase dominate the signal, and if $\phi \simeq 0$ the fluctuations in amplitude dominate the signal. It is not usually possible to establish whether the coherent detectors are measuring phase or amplitude fluctuations at any given time. When the data is analysed it is necessary to be aware that changes in the fluctuation signature could be due to a change from amplitude fluctuations to phase fluctuations or vice versa rather than a physical effect.

The fringe counter data during ELMs show that movements of the reflecting layers correspond to a phase change of $\simeq \pi$. The coherent detector data will thus contain periods with both mainly phase and mainly amplitude fluctuations during an ELM.

The absolute phase, ϕ, will be randomly distributed over the different channels of the reflectometer, and also at the start of separate events on each channel. Thus any observations that are consistent for several channels and several events must be physical phenomena, independent of the absolute phase. The fluctuation characteristics of the ELMs including the outwards movement of the precursor oscillation have been observed in enough cases to be proved physical rather than instrumental.

Density Related Fluctuations during Medium ELMs

Fig.3 shows the fluctuations at several densities in the edge region during one medium and one small ELM. 4-5 ms prior to the larger ELM a high frequency oscillation starts at around $n = 2.5 \times 10^{19} m^{-3}$, and gradually spreads outwards to the rest of the edge region. A similar oscillation also starts 2-3 ms prior to the low amplitude ELM.

Fig.4 shows the autopower spectrum of the density fluctuations vs. time and frequency at four radial positions. A quasi-coherent oscillation at 40-70 kHz (referred to as a precursor) is observed 2-6 ms prior to the D_α burst at both ELMs. The precursor to the larger ELM decreases gradually in frequency towards the ELM. It peaks earlier on the inner channels, suggesting an outward movement of the oscillation. The precursor to the low amplitude ELM does not decrease significantly in frequency, and there is no clear outward movement. At the onset of the main D_α burst a period of enhanced broad-band turbulence is observed for both ELMs. The duration of this coincides with the duration of the D_α burst.

Density Evolution and Fluctuations during Small ELMs

The fluctuation measurements at several densities are shown in fig.5, during a series of small ELMs at the L-H transition. On the top three traces, at $n = 1.4 \times 10^{19} - 2.5 \times 10^{19} m^{-3}$ or $\rho = 0.8 - 0.9$, the density gradient is increasing steadily. The reflecting density layers are moving outwards causing a phase change of several times 2π. This results in a sinusoidal evolution of the reflectometer signals. At densities below $n = 1.1 \times 10^{19} m^{-3}$ outside $\rho = 0.9$ the underlying density profile remains unchanged.

The ELMs are seen as fast changes and oscillations superposed on the base signal, and they are localised to the edge region outside $n = 1.9 \times 10^{19} m^{-3}$. On the top three traces, at densities above $n = 1.4 \times 10^{19} m^{-3}$ the absolute phase at each ELM can be determined from the sinusoidal curve. The perturbation caused by each ELM seems

fairly independent of the absolute phase, ie. whether it is mostly a phase or amplitude perturbation. Furthermore the direction of movement of the reflecting layers during an ELM can be determined; at densities above $n = 1.4x10^{19}m^{-3}$ the ELMs cause a sharp decrease in density followed by slightly slower recovery. At densities below $n = 1.1x10^{19}m^{-3}$ the ELMs result in a sharp increase in density. Here the direction of movement is obtained from fringe counter measurements. The overall effect is a decrease of the density gradient during each ELM.

At the onset of each ELM a burst of oscillations is seen on the traces at $n \leq 1.1x10^{19}m^{-3}$. On one trace only, at $n = 1.1x10^{19}m^{-3}$, one or more bursts of high frequency oscillations are observed prior to each ELM. These precursor oscillations are thus localised to a narrow radial region of < 5 cm. On the traces outside of this, an outward movement of the reflecting density layers is observed during each oscillation burst. This could be due to fluctuation enhanced transport. Another interpretation is also possible; if the precursor before each ELM is continuous but localised to a very narrow region, the observed density layer may be moving in and out in relation to the oscillation, causing it to appear as several separate bursts.

Fig.6 shows the autopower spectrum against time and frequency for $n = 1.1x10^{19}m^{-3}$. One or more quasi-coherent precursor oscillations are seen prior to each ELM, at 60-80 kHz. Each successive precursor before the ELM has a lower peak frequency. Just prior to and coinciding with the D_α burst, a period of broad-band turbulence is observed. Unlike the precursors this is also seen in the rest of the region affected by ELMs.

Density and Magnetic Fluctuations during Large ELMs

Fig.7 shows the autopower spectrum of the density fluctuations at two radial positions in the edge region, and of the fluctuations in $\dot{B}_{pol}$ at the outer midplane, during a large ELM event. At $n = 0.72x10^{19}m^{-3}$ the density fluctuations show a quasi-coherent precursor oscillation at 80-100 kHz, starting $\simeq$20 ms prior to the ELM. Broad-band turbulence is observed just prior to and coinciding with the D_α burst, though at a lower level than the precursor. In the outer edge region the precursor oscillation peaks 2-10 ms prior to the ELM. Further inwards, at $n = 2.5x10^{19}m^{-3}$, the precursor peaks earlier and dies away before the ELM, suggesting an outwards movement of the oscillation. A slight decrease in frequency towards the ELM is also observed, and it is possible that the precursor starts even earlier, but at a higher frequency than the instrumental cut-off at 100 kHz.

The precursor oscillation is also observed on the magnetic field, confirming the reflectometer results. The magnetic precursor seem more continuous. This could be because the magnetic field measurements are not as localised radially as each of the reflectometer channels.

Summary

- The evolution in density gradient and profile in the edge region has been investigated during ELMs using two new techniques for calibrating fixed frequency phase data.
- A significant decrease in density gradient and a density pulse propagating outwards have been observed during the ELM.

- Measurements of density and magnetic fluctuation spectra show a quasi-coherent precursor oscillation prior to the ELM, and a period of broad-band turbulence coinciding with the main D_α burst.
- For larger ELMs the precursor oscillation originates in the inner edge region and spreads outwards. For high frequency, low amplitude ELMs the precursors are localised to one channel only, at $n = 1.1 \times 10^{19} m^{-3}$.
- The problem of whether the coherent detectors at JET are measuring phase or amplitude fluctuations in the reflected signal, depending on the absolute phase, has been addressed. The density related fluctuation signature of the ELMs is shown to be fairly independent of the absolute phase.

Aknowledgements

Lots of thanks to S. Ali-Arshad, D.V. Bartlett, D.J. Campbell, A.E. Costley, G.F. Neill, L. Porte, R. Prentice, and P.E. Stott for help with data collection, discussions and advice.

References

1. K.G. Budden, 'Radio Waves in the Ionosphere', University Press, Cambridge (1961).
2. A.C.C. Sips: 'Reflectometry and Transport in Thermonuclear Plasmas in JET', Phd. Thesis, FOM Institute for Plasma Physics 'Rijnhuizen', NL 1991.
3. A.L. Colton, L. Porte and A.C.C. Sips: 'Measurement Techniques for Plasma Edge Parameters Related to the H-Mode in JET', Proc. 'Contemporary Diagnostics for Fusion Plasmas', Course and Workshop, Varenna, Aug. 1991.

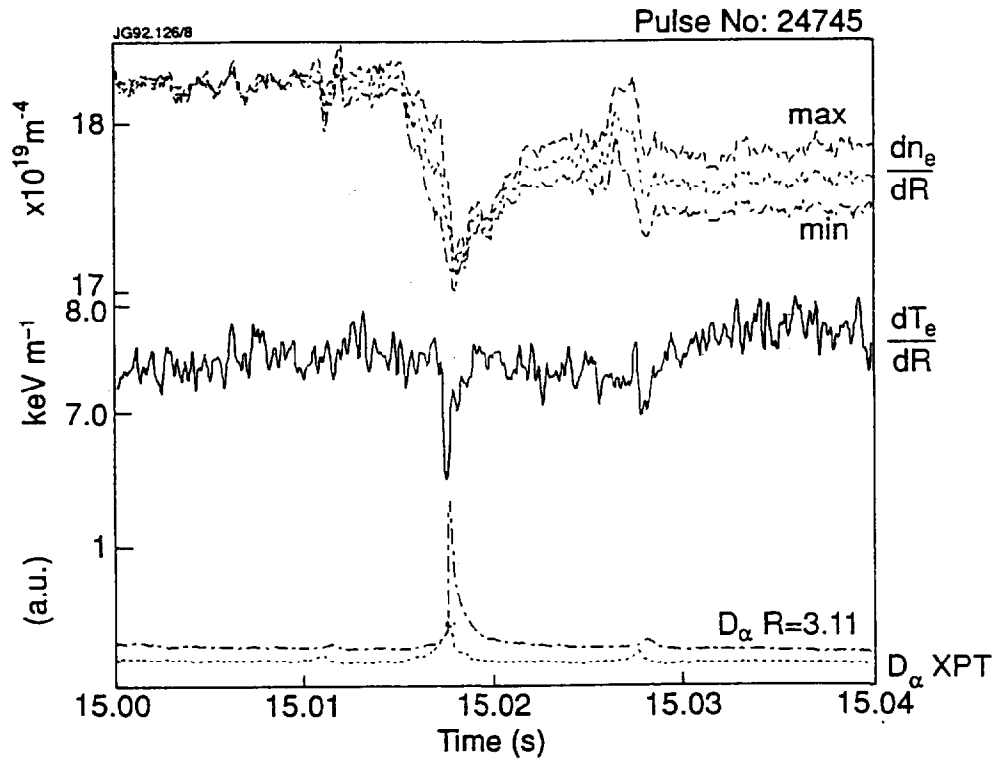

Figure 1: *Density and temperature gradient during medium ELMs.*

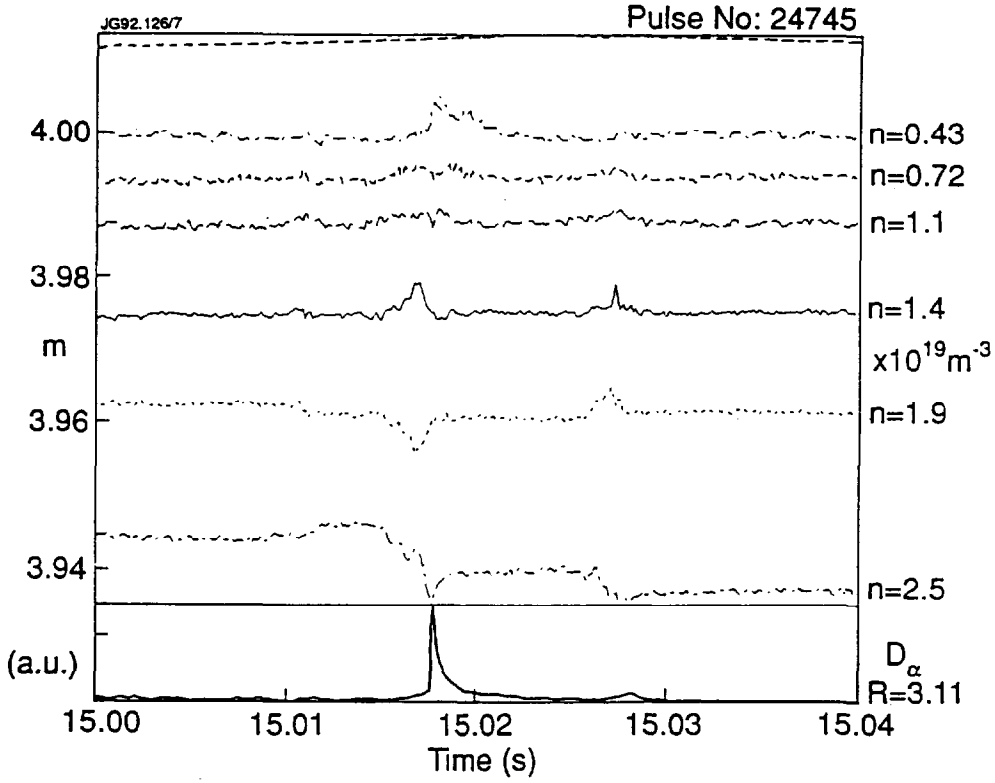

Figure 2: *Density contours during medium ELMs.*

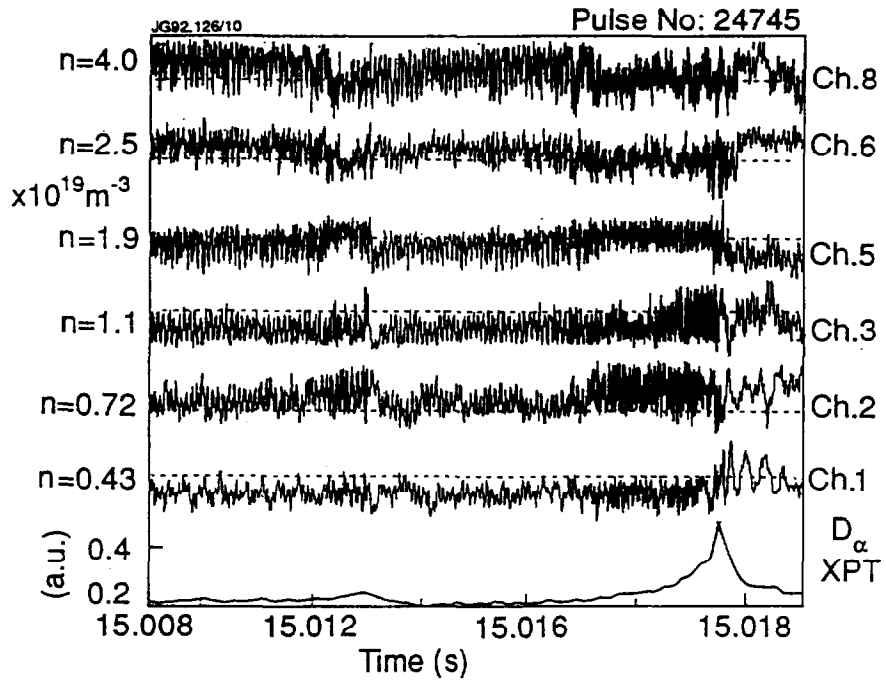

Figure 3 *Density fluctuation measurements during two medium ELMs; high frequency oscillations are seen before each ELM.*

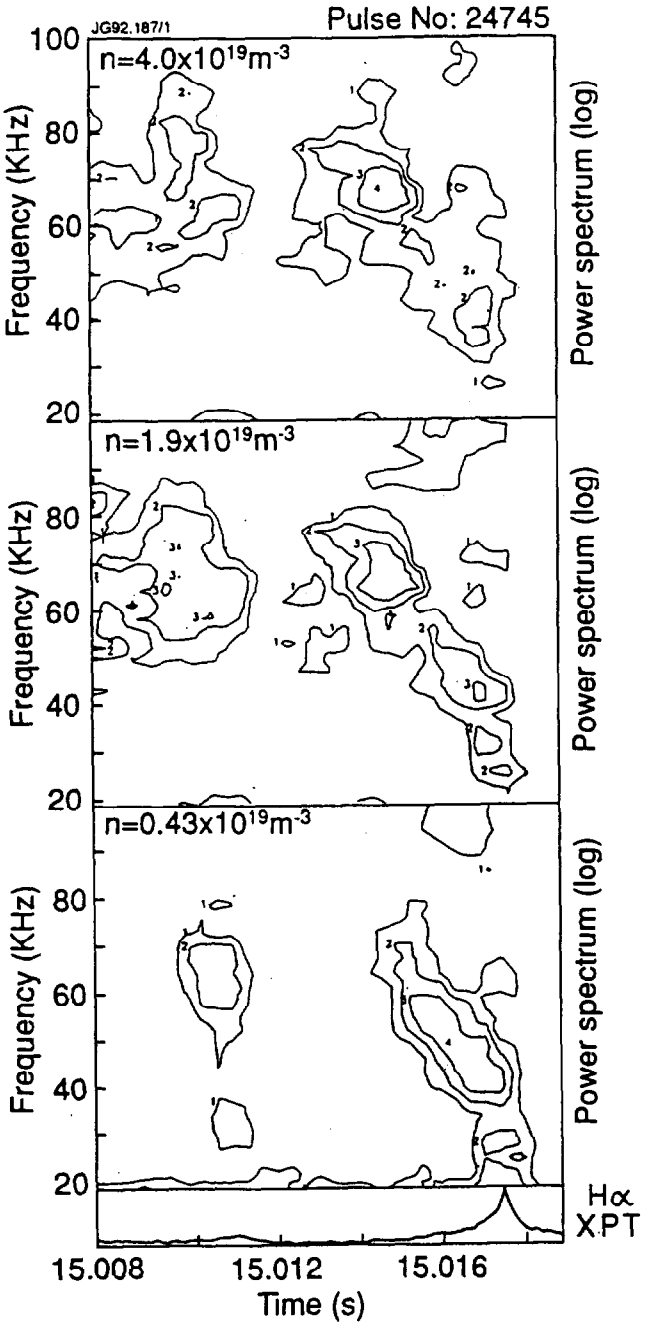

Figure 4 *Autopower spectrum of the density fluctuations in the inner, middle and outer edge region; the precursor to the large ELM peaks 4-5 ms before the D_α burst at the inner position and 0-2 ms before at the outer position.*

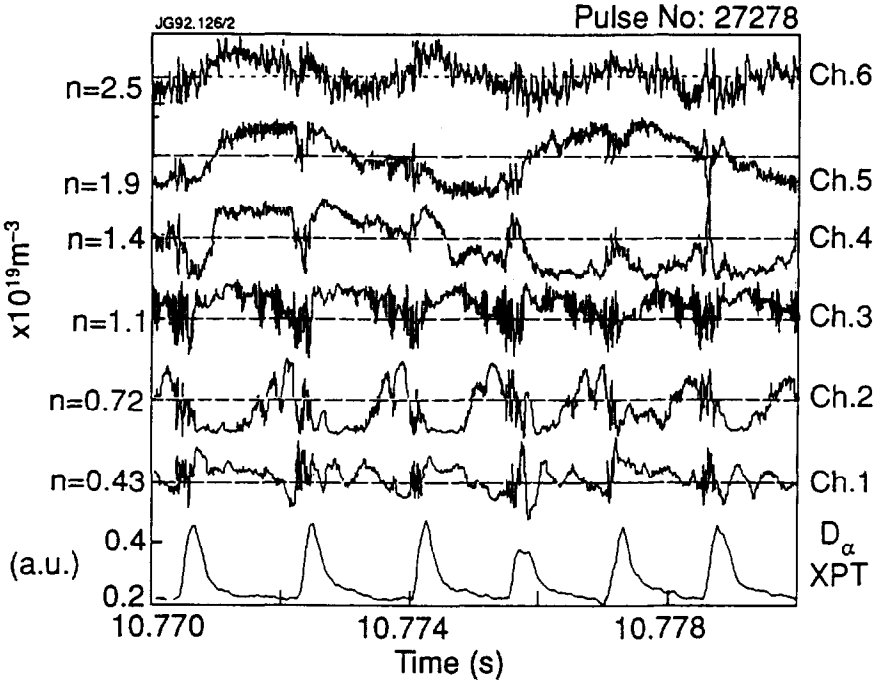

Figure 5: *Density fluctuation measurements during a series of small ELMs at the L-H transition.*

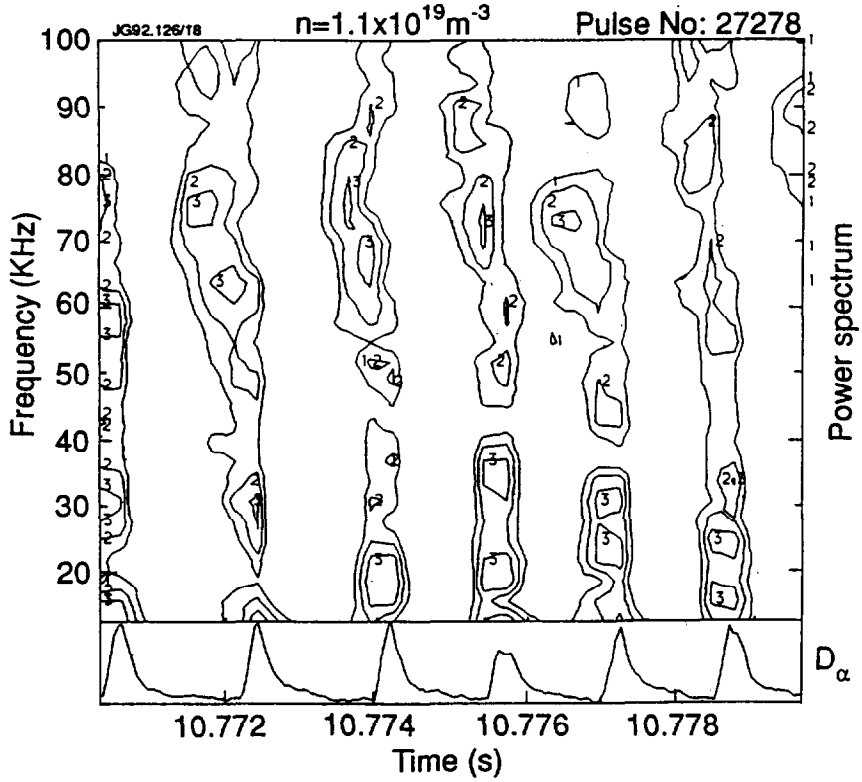

Figure 6: *Autopower spectrum of the fluctuations at* $n = 1.1x10^{19}m^{-3}$.

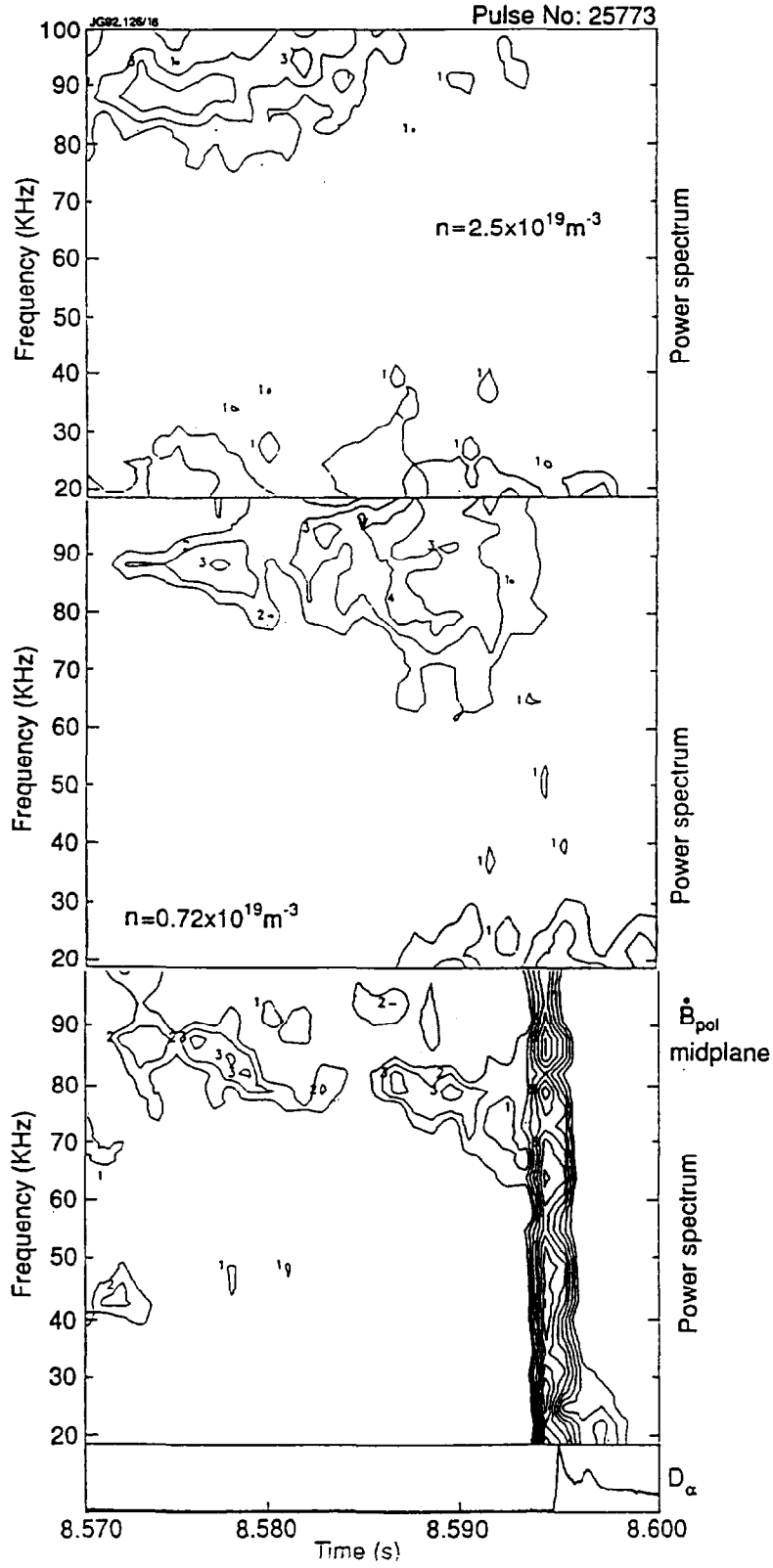

Figure 7: *Autopower spectrum of the density related fluctuations at two densities in the edge region, and of the fluctuations in $\dot{B}_{pol}$ at the outer midplane during a large ELM.*

ANNEX

P.-H. REBUT, A. GIBSON, M. HUGUET, J.M. ADAMS[1], B. ALPER, H. ALTMANN, A. ANDERSEN[2], P. ANDREW[3], M. ANGELONE[4], S. ALI-ARSHAD, P. BAIGGER, W. BAILEY, B. BALET, P. BARABASCHI, P. BARKER, R. BARNSLEY[5], M. BARONIAN, D.V. BARTLETT, L. BAYLOR[6], A.C. BELL, G. BENALI, P. BERTOLDI, E. BERTOLINI, V. BHATNAGAR, A.J. BICKLEY, D. BINDER, H. BINDSLEV[2], T. BONICELLI, S.J. BOOTH, G. BOSIA, M. BOTMAN, D. BOUCHER, P. BOUCQUEY, P. BREGER, H. BRELEN, H. BRINKSCHULTE, D. BROOKS, A. BROWN, T. BROWN, M. BRUSATI, S. BRYAN, J. BRZOZOWSKI[7], R. BUCHSE[22], T. BUDD, M. BURES, T. BUSINARO, P. BUTCHER, H. BUTTGEREIT, C. CALDWELL-NICHOLS, D.J. CAMPBELL, P. CARD, G. CELENTANO, C.D. CHALLIS, A.V. CHANKIN[8], A. CHERUBINI, D. CHIRON, J. CHRISTIANSEN, P. CHUILON, R. CLAESEN, S. CLEMENT, E. CLIPSHAM, J.P. COAD, I.H. COFFEY[9], A. COLTON, M. COMISKEY[10], S. CONROY, M. COOKE, D. COOPER, S. COOPER, J.G. CORDEY, W. CORE, G. CORRIGAN, S. CORTI, A.E. COSTLEY, G. COTTRELL, M. COX[11], P. CRIPWELL[12], O. Da COSTA, J. DAVIES, N. DAVIES, H. de BLANK, H. de ESCH, L. de KOCK, E. DEKSNIS, F. DELVART, G.B. DENNE-HINNOV, G. DESCHAMPS, W.J. DICKSON[13], K.J. DIETZ, S.L. DMITRENKO, M. DMITRIEVA[14], J. DOBBING, A. DOGLIO, N. DOLGETTA, S.E. DORLING. P.G. DOYLE, D.F. DÜCHS, H. DUQUENOY, A. EDWARDS, J. EHRENBERG, A. EKEDAHL, T. ELEVANT[7], S.K. ERENTS[11], L.G. ERIKSSON, H. FAJEMIROKUN[12], H. FALTER, J. FREILING[15], F. FREVILLE, C. FROGER, P. FROISSARD, K. FULLARD, M. GADEBERG, A. GALETSAS, T. GALLAGHER, D. GAMBIER, M. GARRIBBA, P. GAZE, R. GIANNELLA, R.D. GILL, A GIRARD, A. GONDHALEKAR, D. GOODALL[11], C. GORMEZANO, N.A. GOTTARDI, C. GOWERS, B.J. GREEN, B. GRIEVSON, R. HAANGE, A. HAIGH, C.J. HANCOCK, P.J. HARBOUR, T. HARTRAMPF, N.C. HAWKES[11], P. HAYNES[11], J.L. HEMMERICH, T. HENDER[11], J. HOEKZEMA, D. HOLLAND, M. HONE, L. HORTON, J. HOW, M. HUART, I. HUGHES, T.P. HUGHES[10], M. HUGON, Y. HUO[16], K. IDA[17], B. INGRAM, M. IRVING, J. JACQUINOT, H. JAECKEL, J.F. JAEGER, G. JANESCHITZ, Z. JANKOVICZ[18], O.N. JARVIS, F. JENSEN, E.M. JONES, H.D. JONES, L.P.D.F. JONES, S. JONES[19], T.T.C. JONES, J.-F. JUNGER, F. JUNIQUE, A. KAYE, B.E. KEEN, M. KEILHACKER, G.J. KELLY, W. KERNER, A. KHUDOLEEV[21], R. KONIG, A. KONSTANTELLOS, M. KOVANEN[20], G. KRAMER[15], P. KUPSCHUS, R. LÄSSER, J.R. LAST, B. LAUNDY, L. LAURO-TARONI, M. LAVEYRY, K. LAWSON[11], M. LENNHOLM, J. LINGERTAT[22], R.N. LITUNOVSKI, A. LOARTE, R. LOBEL, P. LOMAS, M. LOUGHLIN, C. LOWRY, J. LUPO, A.C. MAAS[15], J. MACHUZAK[19], B. MACKLIN, G. MADDISON[11], C.F. MAGGI[23], G. MAGYAR, W. MANDL[22], V. MARCHESE, G. MARCON, F. MARCUS, J. MART, D. MARTIN, E. MARTIN, R. MARTIN-SOLIS[24], P. MASSMANN, G. MATTHEWS, H. McBRYAN, G. McCRACKEN[11], J. McKIVITT, P. MERIGUET, P. MIELE, A. MILLER, J. MILLS, S.F. MILLS, P. MILLWARD, P. MILVERTON, E. MINARDI[4], R. MOHANTI[25], P.L. MONDINO, D. MONTGOMERY[26], A. MONTVAI[27], P. MORGAN, H. MORSI, D. MUIR, G. MURPHY, R. MYRNÄS[28], F. NAVE[29], G. NEWBERT, M. NEWMAN, P. NIELSEN, P. NOLL, W. OBERT, D. O'BRIEN, J. ORCHARD, J. O'ROURKE, R. OSTROM, M. OTTAVIANI, M. PAIN, F. PAOLETTI, S. PAPASTERGIOU, W. PARSONS, D. PASINI, D. PATEL, A. PEACOCK, N. PEACOCK[11], R.J.M. PEARCE, D. PEARSON[12], J.F. PENG[16], R. PEPE DE SILVA, G. PERINIC, C. PERRY, M. PETROV[21], M.A. PICK, J. PLANCOULAINE, J.-P POFFÉ, R. PÖHLCHEN, F. PORCELLI, L. PORTE[13], R. PRENTICE, S. PUPPIN, S. PUTVINSKII[8], G. RADFORD[30], T. RAIMONDI, M.C. RAMOS DE ANDRADE, R. REICHLE, J. REID, S. RICHARDS, E. RIGHI, F. RIMINI, D. ROBINSON[11], A. ROLFE, R.T. ROSS, L. ROSSI, R. RUSS, P. RUTTER, H.C. SACK, G. SADLER, G. SAIBENE, J.L. SALANAVE, G. SANAZZARO, A. SANTAGIUSTINA, R. SARTORI, C. SBORCHIA, P. SCHILD, M. SCHMID, G. SCHMIDT[31], B. SCHUNKE, S.M. SCOTT, L. SERIO, A SIBLEY, R. SIMONINI, A.C.C. SIPS, P. SMEULDERS, R. SMITH, R. STAGG, M. STAMP, P. STANGEBY[3], R. STANKIEWICZ[32], D.F. START, C.A. STEED, D. STORK, P.E. STOTT, P. STUBBERFIELD, D. SUMMERS, H. SUMMERS[13], L. SVENSSON, J.A. TAGLE[33], M. TALBOT, A. TANGA, A. TARONI, C. TERELLA, A TERRINGTON, A TESINI, P.R. THOMAS, E. THOMPSON, K. THOMSEN, F. TIBONE, A. TISCORNIA, P. TREVALION, B. TUBBING, P. VAN BELLE, H. VAN DER BEKEN, G. VLASES, M. VON HELLERMANN, T. WADE, C. WALKER, R. WALTON[31], D. WARD, M.L. WATKINS, N. WATKINS, M.J. WATSON, S. WEBER[34], J. WESSON, T.J. WIJNANDS, J. WILKS, D. WILSON, T. WINKEL, R. WOLF, D. WONG, C. WOODWARD, Y. WU[35], M. WYKES, D. YOUNG, I.D. YOUNG, L. ZANNELLI, A. ZOLFAGHARI[19], W. ZWINGMANN

[1] Harwell Laboratory, UKAEA, Harwell, Didcot, Oxfordshire, UK.
[2] Risø National Laboratory, Roskilde, Denmark.
[3] Institute for Aerospace Studies, University of Toronto, Downsview, Ontario, Canada.
[4] ENEA Frascati Energy Research Centre, Frascati, Rome, Italy.
[5] University of Leicester, Leicester, UK.
[6] Oak Ridge National Laboratory, Oak Ridge, TN, USA.
[7] Royal Institute of Technology, Stockholm, Sweden.
[8] I.V. Kurchatov Institute of Atomic Energy, Moscow, Russian Federation.
[9] Queens University, Belfast, UK.
[10] University of Essex, Colchester, UK.
[11] Culham Laboratory, UKAEA, Abingdon, Oxfordshire, UK.
[12] Imperial College of Science, Technology and Medicine, University of London, London, UK.
[13] University of Strathclyde, Glasgow, UK.
[14] Keldysh Institute of Applied Mathematics, Moscow, Russian Federation.
[15] FOM-Institute for Plasma Physics "Rijnhuizen", Nieuwegein, Netherlands.
[16] Institute of Plasma Physics, Academia Sinica, Hefei, Anhui Province, China.
[17] National Institute for Fusion Science, Nagoya, Japan.
[18] Soltan Institute for Nuclear Studies, Otwock/Świerk, Poland.
[19] Plasma Fusion Center, Massachusetts Institute of Technology, Boston, MA, USA.
[20] Nuclear Engineering Laboratory, Lappeenranta University, Finland.
[21] A.F. Ioffe Physico-Technical Institute, St. Petersburg, Russian Federation.
[22] Max-Planck-Institut für Plasmaphysik, Garching, Germany.
[23] Department of Physics, University of Milan, Milan, Italy.
[24] Universidad Complutense de Madrid, Madrid, Spain.
[25] North Carolina State University, Raleigh, NC, USA.
[26] Dartmouth College, Hanover, NH, USA.
[27] Central Research Institute for Physics, Budapest, Hungary.
[28] University of Lund, Lund, Sweden.
[29] Laboratorio Nacional de Engenharia e Tecnologia Industrial, Sacavem, Portugal.
[30] Institute of Mathematics, University of Oxford, Oxford, UK.
[31] Princeton Plasma Physics Laboratory, Princeton University, Princeton, NJ, USA.
[32] RCC Cyfronet, Otwock/Świerk, Poland,
[33] Centro de Investigaciones Energéticas, Medioambientales y Tecnológicas, Madrid, Spain.
[34] Freie Universität, Berlin, Germany.
[35] Insitute for Mechanics, Academia Sinica, Beijing, China.